ARTICLE

Experimental Determination of Single CdSe Nanowire Absorption Cross Sections through Photothermal Imaging

Jay Giblin,[†] Muhammad Syed,[‡] Michael T. Banning,[†] Masaru Kuno,[†,*] and Greg Hartland[†]

[†]Department of Chemistry and Biochemistry, University of Notre Dame, 251 Nieuwland Science Hall, Notre Dame, Indiana 46556, and [‡]Nanotechnology Engineering, University of Waterloo, Waterloo, Ontario, Canada, N2L 3G1

ABSTRACT Absorption cross sections (σ_{abs}) of single branched CdSe nanowires (NWs) have been measured by photothermal heterodyne imaging (PHI). Specifically, PHI signals from isolated gold nanoparticles (NPs) with known cross sections were compared to those of individual CdSe NWs excited at 532 nm. This allowed us to determine average NW absorption cross sections at 532 nm of $\sigma_{abs} = (3.17 \pm 0.44) \times 10^{-11}$ cm^2/μm (standard error reported). This agrees well with a theoretical value obtained using a classical electromagnetic analysis ($\sigma_{abs} = 5.00 \times 10^{-11}$ cm^2/μm) and also with prior ensemble estimates. Furthermore, NWs exhibit significant absorption polarization sensitivities consistent with prior NW excitation polarization anisotropy measurements. This has enabled additional estimates of the absorption cross section parallel ($\sigma^{\parallel}_{abs}$) and perpendicular ($\sigma^{\perp}_{abs}$) to the NW growth axis, as well as the corresponding NW absorption anisotropy (ρ_{abs}). Resulting values of $\sigma^{\parallel}_{abs} = (5.6 \pm 1.1) \times 10^{-11}$ cm^2/μm, $\sigma^{\perp}_{abs} = (1.26 \pm 0.21) \times 10^{-11}$ cm^2/μm, and $\rho_{abs} = 0.63 \pm 0.04$ (standard errors reported) are again in good agreement with theoretical predictions. These measurements all indicate sizable NW absorption cross sections and ultimately suggest the possibility of future *direct* single NW absorption studies.

KEYWORDS: nanowire · photothermal microscopy · CdSe · absorption cross section · gold nanoparticles · solution−liquid−solid growth · absorption polarization anisotropy

The absorption cross section (σ_{abs}) is a fundamental property of molecules and nanoparticles. For systems with well-defined molecular weights, σ_{abs} can be determined with relative ease using absorption spectroscopy along with the Beer−Lambert law. However, extracting σ_{abs} for nanostructures such as colloidal quantum dots (QDs) and nanowires (NWs) is not straightforward because of the existence of sample polydispersities. Even the best preparations result in radius distributions ranging from 4 to 10% in QDs and 15 to 30% in NWs.[1−14] Current syntheses also do not control NW lengths. Adding to this, organic surfactants bound to the surface of chemically grown QDs and NWs prevent accurate measurement of their true masses. As a consequence, it is difficult to associate a specific molecular weight or sample concentration to chemically grown nanostructures.

While there has been much recent work to ascertain QD σ_{abs} values,[15−17] these numbers are still being vetted for NWs. It is important to substantiate this optical parameter since knowledge of σ_{abs} enables more accurate estimates of NW concentrations, emission quantum yields, photodetector conversion efficiencies, external photovoltaic efficiencies, as well as lasing thresholds. However, despite this need, we are only aware of three studies on the subject.[18−20] Experimental ensemble CdSe and CdTe NW σ_{abs} values across the visible were first reported in ref 18, using correlated transmission electron microscopy, UV/visible extinction spectroscopy, and inductively coupled plasma atomic emission spectroscopy. At the same time, ref 19 employed a back of the envelope expression to estimate single CdSe NW σ_{abs} values at wavelengths far to the blue of the band edge, while ref 20 used a classical Poynting vector analysis to treat the linear absorption of NWs. Given the existence of significant size and/or morphology (branching) distributions in current samples, motivation exists for measurements of *single* NW absorption cross sections.

In this article, we demonstrate the ability to determine single CdSe NW σ_{abs} values using photothermal heterodyne imaging (PHI). This sensitive single molecule detection technique has previously been used to study the absorption of Au nanoparticles (NPs),[21,22] core/shell CdSe/ZnS quantum dots,[23] and single-walled carbon nanotubes.[24,25] The technique indirectly measures optical absorption by monitoring the heat dissipated to the local environment around an absorbing object. Specifically, a modulated heating beam creates a time-varying refractive index in the object's

*Address correspondence to mkuno@nd.edu.

Received for review September 7, 2009 and accepted December 22, 2009.

Published online January 4, 2010. 10.1021/nn901172s

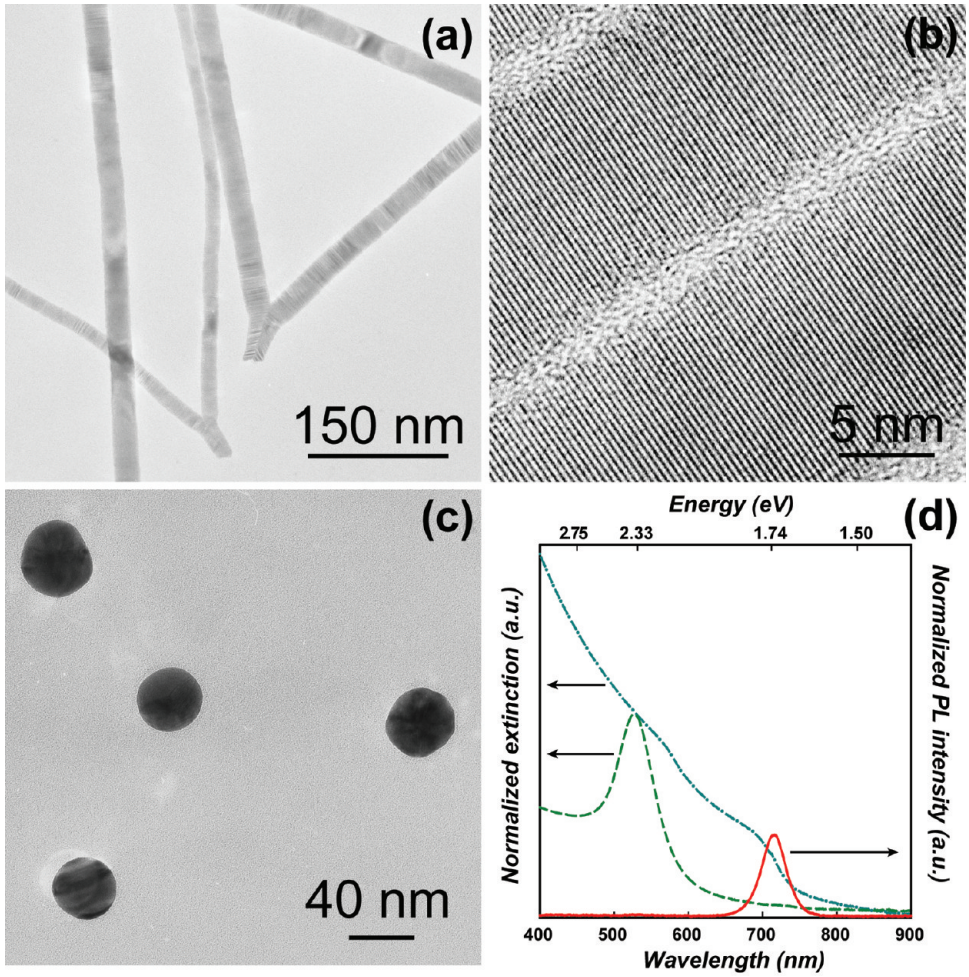

Figure 1. Representative (a) low and (b) high resolution TEM images of CdSe NWs with (c) accompanying low resolution TEM images of Au NPs. (d) Linear extinction spectra of CdSe NW (dashed-dotted line) and Au NP (dashed line) ensembles with the corresponding NW band edge photoluminescence (PL) (solid line) shown.

environment that is subsequently detected though changes in the propagation of a nonresonant probe beam. The method works best in systems that relax quickly to the ground state (nonradiatively), allowing fast excitation cycling. Reference 26 more fully explains the PHI technique.

RESULTS AND DISCUSSION

Given that individual NWs typically exhibit low emission quantum yields (QYs),[19,27−30] they represent a good candidate system for photothermal imaging. In the specific case of CdSe, QYs are estimated to be on the order of 0.1%.[19] While there have been some exceptions to this,[29,30] such low emission efficiencies indicate that these wires effectively dissipate any absorbed energy as heat into the surrounding environment. We have therefore used PHI to image and measure the absorption cross sections of individual CdSe NWs at 532 nm (2.33 eV). The cross-section measurement relies on comparing the magnitude of the PHI signal for the NWs to those of Au NPs with a well-defined size.[31,25]

Branched CdSe NWs were prepared *via* solution−liquid−solid growth, the details of which can be found in ref 9. Figure 1 shows low (panel a) and high resolution (panel b) transmission electron microscopy (TEM) images of resulting wires. The TEM micrographs reveal that the wires are highly crystalline with lengths between 1 and 10 μm and with an average radius of 10.9 ± 4.3 nm. Obtained NW morphologies include v-shape, y-shape, and "merge-y" geometries.[9] Cartoon schematics, providing more details about these NW structures, can be found in the Supporting Information as well as in ref 9. The gold particles used in this study were synthesized using a radiolytic method developed by Henglein.[32] The resulting average particle radius is 21.1 ± 1.8 nm (Figure 1c). Reported errors in both CdSe NW and Au NP sizes represent one standard deviation about the mean. Both nanostructures absorb at 532 nm, as illustrated in Figure 1d. Given that the Au NP σ_{abs} value at 532 nm is well-known, single CdSe NW σ_{abs} values can be determined by comparing the integrated PHI signal per micrometer for the NWs to the signal from the NPs.

Samples for optical measurements were prepared by spin-coating dilute solutions of CdSe NWs or Au NPs onto flamed glass microscope coverslips. To

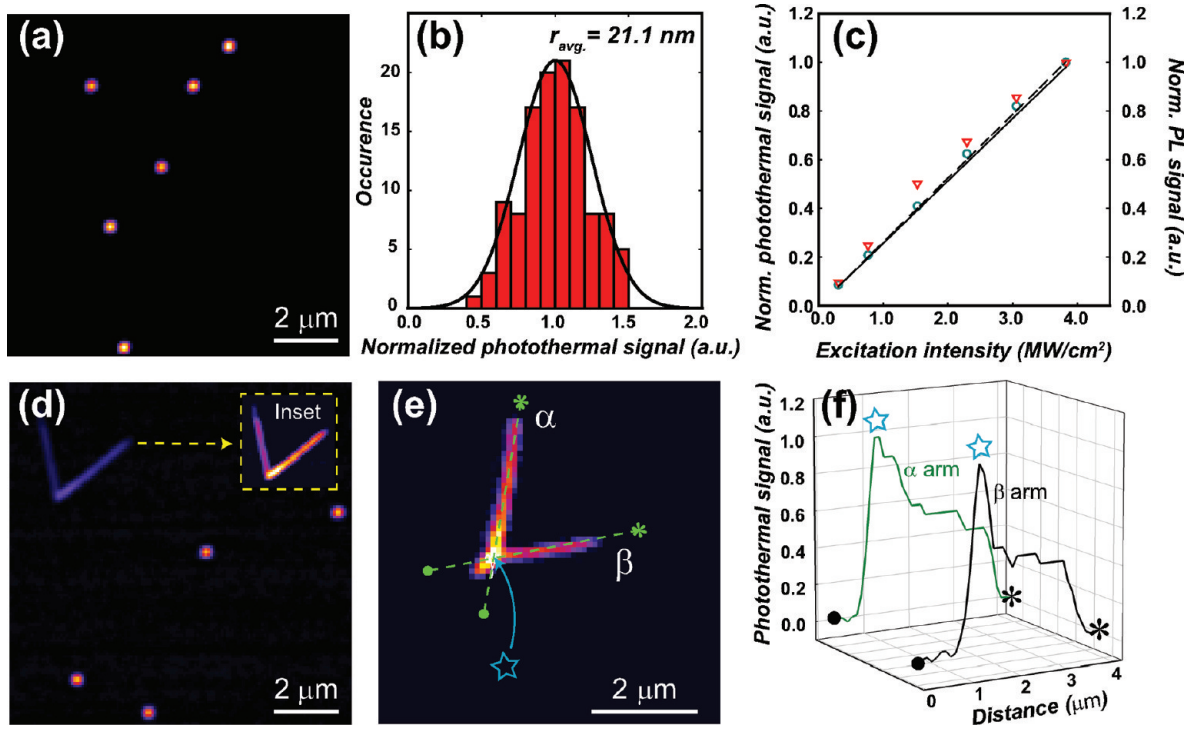

Figure 2. (a) Photothermal image of evenly dispersed single Au NPs within a 6.4 × 6.4 μm² region. (b) Histogram of integrated PHI values normalized to the mean of 117 individual Au NPs. The solid Gaussian curve illustrates the corresponding Au NP volume distribution determined by TEM. (c) NW PHI (open circles) and PL (open triangles) intensity as a function of excitation intensity. The solid/dashed lines are linear fits to each data set. (d) Photothermal image of a single v-shape NW from a 6.4 × 6.4 μm² region with Au NPs present. (e) Photothermal image of a single merge-y NW from a 6.4 × 6.4 μm² region with (f) the corresponding intensity profile of arms α and β. Open stars denote the merge-y branching point.

ensure that only single NWs were studied, wires with characteristic v-shape, y-shape, and merge-y morphologies (as opposed to straight NWs) were chosen for these experiments. In parallel, gold particle solutions were diluted until interparticle distances of at least 0.5 μm were achieved on the glass coverslip and PHI signals were uniform from particle-to-particle, as demonstrated in Figure 2a. A histogram of the integrated photothermal signal from 117 Au NPs (Figure 2b) reveals a monomodal distribution, suggesting the successful detection of single Au particles. The solid line represents the corresponding Au NP volume distribution (assumed to be Gaussian) determined from TEM analysis. By comparing the relative standard deviation in the distribution for the Au photothermal signal (22%) to that of the NP volume (25%), we conclude that the spread in the PHI signal arises from the sample size distribution.[26]

As a further control experiment, single NW PHI and photoluminescence (PL) signals were measured as a function of excitation intensity. In both cases, a linear dependence was seen within the range of excitation intensities used (~300 kW/cm² to 4 MW/cm²) (Figure 2c). The lack of any saturation behavior implies that the PHI signals from the Au NPs and CdSe NWs can be directly compared. Note that all subsequent measurements were conducted in the low excitation regime of the heating beam (~180 kW/cm²). A typical photothermal image of a single y-shape NW with Au NPs present is shown in Figure 2d. Circularly polarized light was used in this measurement. The Au particles appear brighter than the CdSe NW in the image, suggesting that they have larger cross sections. A more quantitative analysis of this difference follows.

Figure 2d,e illustrates variations in the PHI signal for different arms of a given NW, again recorded with circularly polarized light. This is attributed to the distribution of widths from arm-to-arm (the relative standard deviation in the width is 40%). Interestingly, of the six total branched wires imaged, an intrawire analysis suggests that the PHI signal is greatest near their branching point. Figure 2f demonstrates this by plotting the PHI profile of arms α and β from the merge-y NW shown in Figure 2e. This behavior could be due to two effects. It may arise from an increase in the incident electric field strength at the branching point, which results in an increase of the absorption.[33] Another possibility is that at branching points we simply interrogate more material within our diffraction limited spot.

In total, 12 arms from 6 NWs were analyzed using circularly polarized light, and each arm was treated as a separate measurement. The relative absorption cross section of each arm was obtained by integrating the PHI signal over the entire arm, excluding branching points, and dividing by its length. The effect of the increased PHI signal near branching points (Figure 2f) only increases the obtained cross section by 10% at most. This

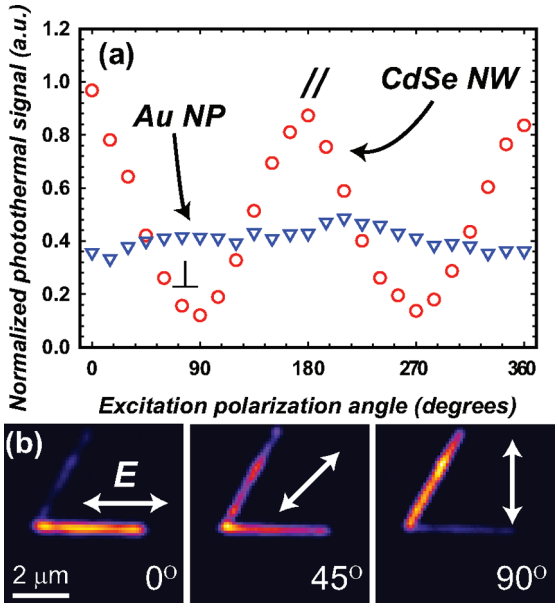

Figure 3. (a) Single NW (open circles) and Au NP (triangles) PHI signals plotted against excitation polarization angle relative to the NW growth axis. (b) Corresponding NW PHI images at fixed angles (λ_{exc}= 532 nm).

is overshadowed by larger sources of error as will be discussed below.

A comparison to the integrated signal from 117 Au NPs then reveals that, on average, the NW PHI signal per micrometer is 0.58 times less than the Au NP signal. An absolute value of σ_{abs} was then obtained by multiplying this ratio with the Mie theory calculated absorption cross section for 21.1 nm Au NPs ($\sigma_{abs} = 5.61 \times 10^{-11}$ cm^2, $\lambda_{exc} = 532$ nm) (Supporting Information). Note that our experiments were performed using microscope immersion oil to index match the second objective and to dissipate any heat generated by the NPs or NWs. As a consequence, the refractive index of oil ($n = 1.51$) was used in the Mie theory calculation. Furthermore, in these calculations the complex refractive index of Au at 532 nm from ref 34 was used ($0.523 - i2.227$), without any corrections for electron surface scattering.[35] The end result of this analysis is an average CdSe NW absorption cross section of σ_{abs}= (3.17 ± 0.44) $\times 10^{-11}$ cm^2/μm (standard error reported) for excitation with 532 nm, circularly polarized light.

It is well-documented that the absorption of NWs possesses strong excitation polarization sensitivities.[36,37] Consequently, in addition to circularly polarized light, single NWs were excited with parallel and perpendicularly polarized light relative to the growth axis of each arm. Figure 3a demonstrates that the intensity of the PHI signal from an individual branched NW arm depends strongly on the incident light's polarization angle. Clear oscillations occur as a function of the polarization angle with the signal maximized when the excitation is parallel to the NW growth axis. Figure 3b shows sequential PHI images taken at 0, 45, and 90° relative to an arm of a y-shape NW that further demonstrate this effect. For completeness, Figure 3a also shows that gold NPs do not exhibit any significant polarization sensitivities, as expected. An absorption anisotropy (ρ_{abs}) averaged over 7 NW arms is $\rho_{abs} = 0.63 \pm 0.04$ (standard error reported) in good agreement with the value expected for an immersion oil environment as calculated below (theoretical $\rho_{abs} = 0.66$).[20]

Comparison of the integrated PHI signal per micrometer (from 7 single NW arms excited with parallel excitation) to that of the 21.1 nm radius Au NPs reveals an approximate 1:1 ratio. For perpendicularly polarized light, it is 1:4.45. On the basis of the above calculated σ_{abs} value for Au NPs as well as the ratio of the NW-to-NP PHI signal, average parallel/perpendicular cross sections are then $\sigma^{\parallel}_{abs} = (5.61 \pm 1.12) \times 10^{-11}$ cm^2/μm and $\sigma^{\perp}_{abs} = (1.26 \pm 0.21) \times 10^{-11}$ cm^2/μm (standard errors reported). We note that it is experimentally more challenging to obtain $\sigma^{\parallel}_{abs}$ and $\sigma^{\perp}_{abs}$ values compared to finding σ_{abs} for circularly polarized light since the presence of a beam splitter prior to the microscope objective leads to an unavoidable scrambling of the excitation polarization at orientations other than s or p (see Supporting Information Figure S.1). Thus, only NW arms already possessing an s or p orientation relative to the beam splitter could be used for these experiments. This limited the total number of measurements conducted.

Experimentally determined σ_{abs}, $\sigma^{\parallel}_{abs}$, and $\sigma^{\perp}_{abs}$ values were compared to results of a predictive NW cross-section method developed earlier.[20] The technique is based on the analytical determination of the total optical power absorbed by a unit NW length of radius a in a nonabsorbing medium with dielectric constant ε_M. Additional details of the method can be found in ref 20. However, the model ultimately yields the following absorption cross sections:

$$\sigma^{\parallel}_{abs}(\omega) = \frac{2\pi a}{Z\varepsilon_M v}\mathrm{Re}\left\{-i\sum_{n=-\infty}^{\infty}\sqrt{\varepsilon(\omega)}^{*}|c_n|^2 J_n(ka)J_n'^{*}(ka)\right\} \quad (1)$$

and

$$\sigma^{\perp}_{abs}(\omega) = \frac{2\pi a}{Z\varepsilon_M v}\mathrm{Re}\left\{i\sum_{n=-\infty}^{\infty}\sqrt{\varepsilon(\omega)}^{*}|d_n|^2 J_n'(ka)J_n^{*}(ka)\right\} \quad (2)$$

for excitation at a wavelength λ, polarized parallel and perpendicular to the NW growth axis. In either expression, Z is the wave impedance of free space ($Z = (\mu_0/\varepsilon_0)^{1/2}$), μ_o (ε_o) is the permeability (permittivity) of free space, $k = (\varepsilon(\omega))^{1/2}2\pi/\lambda$ is the wavenumber inside the NW, $\varepsilon(\omega)$ is the NW's complex frequency-dependent dielectric constant, v is the speed of the wave in the surrounding medium, and $J_n(kr)$ are Bessel functions of the first kind with J_n'(kr) their first derivatives. The expansion coefficients c_n and d_n, in a nonabsorbing medium, are

$$c_n = \frac{\sqrt{\varepsilon_M}H_n'(k_0a)J_n(k_0a) - \sqrt{\varepsilon_M}H_n(k_0a)J_n'(k_0a)}{\sqrt{\varepsilon_M}H_n'(k_0a)J_n(ka) - \sqrt{\varepsilon(\omega)}H_n(k_0a)J_n'(ka)} \quad (3)$$

$$d_n = \frac{\sqrt{\varepsilon_M}H_n(k_0a)J_n'(k_0a) - \sqrt{\varepsilon_M}J_n(k_0a)H_n'(k_0a)}{\sqrt{\varepsilon_M}J_n'(ka)H_n(k_0a) - \sqrt{\varepsilon(\omega)}J_n(ka)H_n'(k_0a)} \quad (4)$$

where $H_n(k_0a)$ are complementary Hankel functions of the first kind, $H_n'(kr)$ are their first derivatives, and $k_0 = ((\varepsilon_M)^{1/2}2\pi)/\lambda$ is the wavenumber in the surrounding medium. For circularly polarized light, σ_{abs} is given by[38]

$$\sigma_{abs} = \frac{\sigma_{abs}^{\parallel} + \sigma_{abs}^{\perp}}{2} \quad (5)$$

Evaluation of eq 5, along with eqs 1−4, yields $\sigma_{abs} = 5.00 \times 10^{-11}$ cm^2/μm for a 10.9 nm radius CdSe NW in an immersion oil environment ($\lambda_{exc} = 532$ nm). Furthermore, given $\sigma_{abs}^{\parallel}$ and $\sigma_{abs}^{\perp}$, the following expression for the absorption polarization anisotropy, $\rho_{abs} = (\sigma_{abs}^{\parallel} - \sigma_{abs}^{\perp})/(\sigma_{abs}^{\parallel} + \sigma_{abs}^{\perp})$, leads to a theoretical absorption anisotropy of $\rho_{abs} = 0.66$. In all cases, given the absence of actual NW $\varepsilon(\omega)$ values, the bulk frequency-dependent dielectric constant of CdSe was used.[39] Mathematica code for the above calculation can be found in the Supporting Information. The results calculated using eqs 1−5 are in reasonable agreement with experimental σ_{abs}, $\sigma_{abs}^{\parallel}$, $\sigma_{abs}^{\perp}$, and ρ_{abs} values, as illustrated in Table 1. Variations in reported NW absorption cross sections arise mainly due to structural variations in the NW, specifically, inter-arm variations (in our case 40% as reported above) and intra-arm radius variations (reported in the literature as ∼5%).[9]

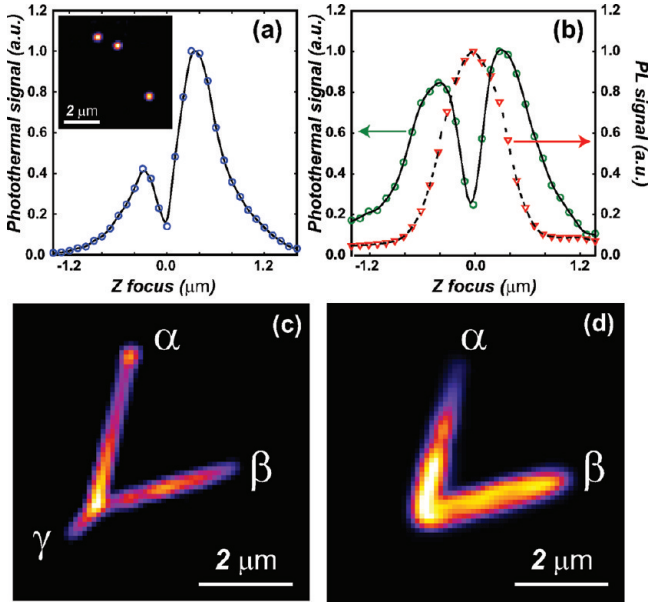

Figure 4. Photothermal signal of a single (a) Au NP and (b) a CdSe NW (open circles) with the corresponding NW PL intensity (triangles). All data are plotted as a function the objective's z-position relative to the coverslip. The solid/dashed lines in (a) and (b) are guides to the eye. Corresponding images: (c) PHI and (d) PL. Greek letters denote different arms of the branched NW.

TABLE 1. Reported (10.9 nm radius) CdSe NW Absorption Cross Sections and the Associated Absorption Polarization Anisotropy at 532 nm (Standard Errors Are Reported)

	experimental	calculated
σ_{abs}	3.17×10^{-11} cm^2/μm (±14%)	5.00×10^{-11} cm^2/μm
$\sigma_{abs}^{\parallel}$	5.61×10^{-11} cm^2/μm (±20%)	8.29×10^{-11} cm^2/μm
$\sigma_{abs}^{\perp}$	1.26×10^{-11} cm^2/μm (±17%)	1.72×10^{-11} cm^2/μm
ρ_{abs}	0.63 (±6%)	0.66

Note that typical PHI experiments utilize a probe beam off-resonance with the studied material. However, our measurement employs a red 632.8 nm probe, which is resonant with the interband absorption of the CdSe NWs (Figure 1). On the basis of the calculated CdSe NW σ_{abs} value at this wavelength (Supporting Information), only ∼1.2% of the probe power is absorbed. This corresponds to a negligible difference in the recorded PHI signal and therefore allows us to compare the signal measured from CdSe NWs to those of Au NPs in order to extract relevant NW absorption cross sections.

Finally, while adjusting the PHI signal in the single CdSe NW and Au NP experiments, two maxima in the signal were observed at different positions of the focusing objective relative to the coverslip surface. This is shown in Figure 4a for a single Au NP and in Figure 4b for a single CdSe NW (open circles). Hwang and Moerner have previously examined (theoretically) the far-field signal induced by a nanoparticle in a focused Gaussian laser beam, as a function of the particle's position relative to the focal plane.[40] This signal can arise from an absorption or a phase change of the beam. For an experiment where absorption dominates, the signal is maximized at the focus. In contrast, when the phase change contribution dominates, the signal is minimized at the focus and displays two maxima symmetrically distributed about it, separated by roughly the Rayleigh range of the beam. This effect arises from the Gouy phase change of the Gaussian beam as it passes through a focus.[40] In PL experiments, the signal is due to photon absorption and should therefore display a single maximum at exactly the beam focus. Since single NP/NW PHI experiments are sensitive to changes in the refractive index of the environment caused by heating, this corresponds to the latter phase change scenario and thus means that two maxima should be observed when a particle/NW is scanned through the focus.

Figure 4b illustrates the difference between absorption and emission by plotting the PHI signal and PL intensity of a single NW as function of the objective's z-position relative to the coverslip. It can be seen that the PHI signal for the NWs displays two maxima, with a minimum at the point where the PL signal is maximized. The PHI signal for the Au NPs also displays two maxima, but the intensities in this case are very

asymmetric. In the context of the Hwang and Moerner paper, asymmetry arises when the signal detected originates from a mixture of absorption and phase changes. Note that the degree of asymmetry in the PHI signal for both the NPs and NWs varies from particle to particle. In light of this, to ensure consistency in our PHI measurements, care was taken to always maximize the signal by positioning the objective at the larger of the two photothermal peaks. Emission images were likewise acquired by adjusting the z-position of the objective to maximize the emission intensity. As a consequence of the asymmetry in the PHI signal, a systematic error ultimately exists in determined NW absorption cross sections. Unfortunately, it is difficult to quantify an exact correction factor because the interplay between absorption and phase change effects is intrinsically complicated.[40] However, we believe that obtained NW cross sections are likely underestimated by ~10−20% and this, in turn, might explain the systematically smaller experimental *versus* theoretical values in Table 1. This subtle effect thus brings us to the conclusion that direct absorption measurements of NW absorption cross sections will yield more accurate results.[41]

As a final point of interest, Figure 4c shows that in the specific case of merge-y NWs, when the NW PHI signal is maximized, all three arms, α, β, and γ, are visible. However, when the corresponding PL signal is maximized, only two arms (α,β) are apparent with the third arm (γ) absent (Figure 4d). This was not exclusive to the particular wire shown and was observed for all merge-y NWs studied. A possible explanation is that the high angle grain boundary running down the length of the γ arm (see Supporting Information and ref 9) causes rapid nonradiative recombination of electrons and holes, quenching the emission.

CONCLUSION

In conclusion, single branched CdSe NWs were studied using photothermal heterodyne imaging. Experiments reveal variations in NW absorption along the length of each arm with the greatest absorption occurring near branching points. Absolute CdSe NW σ_{abs} values for circular, parallel, and perpendicularly polarized light at 532 nm were determined by comparing the PHI signal of NWs to those of Au NPs. Obtained cross sections were in good agreement with calculated values using the bulk dielectric constant of CdSe. In addition, extracted *absorption* polarization anisotropy values agree well with prior experimental and theoretical excitation polarization anisotropies. These large σ_{abs} and ρ_{abs} values suggest the possibility of future direct single NW absorption measurements. Furthermore, these spatially resolved measurements also show that absorption and emission are not perfectly correlated in single nanowires. For example, in "merge-y" nanowires the "γ-arm" clearly can be seen in absorption but not emission (see Figures 4b,c). This appears to be due to an increased nonradiative recombination of electrons and holes in this arm due to structural defects in the wire.[9]

EXPERIMENTAL SECTION

Photothermal measurements were preformed using a home-built single molecule imaging instrument, based on an inverted optical microscope (Olympus IX-71). NW and gold NP positions were manipulated using a manual X-Y micrometer stage (Semprex) coupled to a closed-loop, three-axis piezo positioner (Physik Instrumente, P-527.3Cl). The experiments employed a 632.8 nm HeNe probe beam (JDS Uniphase) overlaid on a 532 nm heating beam (Spectra Physics, Millennia Vs). The intensity of the latter was modulated at 100 kHz using a photoelastic modulator (Hinds Instruments). The heating and probe beams were focused on the sample using a high numerical aperture (NA) oil-immersion objective (Olympus, 100×/1.30 NA), with excitation intensities of ~180 and ~20 kW/cm^2, respectively (calculated assuming diffraction-limited excitation spots of $d = \lambda/(2\mathrm{NA})$. The pump and probe beams were subsequently recollimated with a second oil-immersion objective (Olympus, 60×/0.9 NA), whereupon the green heating beam was eliminated using a 633 nm band-pass filter (Semrock). The red probe was subsequently detected with an avalanche photodiode module (Hamamatsu C5331−11) coupled to a lock-in amplifier (Stanford Research Systems SR830). NW emission was simultaneously collected with the first microscope objective and was filtered through a 710 nm long pass filter (Chroma) before being detected using a fiber coupled, single photon counting avalanche photodiode (Perkin-Elmer SPCM-AQR-14). Photothermal and emission images were created by raster scanning the sample using in-house software. A detailed diagram of the experimental setup can be found in the Supporting Information (Figure S.1).

Acknowledgment. G.H. acknowledges support from the National Science Foundation (Grant CHE06-47444), and the University of Notre Dame Faculty Research Program. M.K. thanks the NSF CAREER program (CHE-0547784), the Notre Dame Radiation Laboratory, and the DOE Office of Basic Energy Sciences for financial support as well as access to their equipment and facilities. M.K. is a Cottrell Scholar of Research Corporation.

Supporting Information Available: Detailed experimental diagram. Sample Au NP absorption cross-section calculation. Sample CdSe NW absorption cross-section calculation. Calculation of 633 nm probe power absorbed by a CdSe NW. Cartoon schematic of branched NW morphologies. This material is available free of charge *via* the Internet at http://pubs.acs.org.

REFERENCES AND NOTES

1. Peng, Z. A.; Peng, X. G. Formation of High-Quality CdTe, CdSe, and CdS Nanocrystals Using CdO as Precursor. *J. Am. Chem. Soc.* **2001**, *123*, 183–184.
2. Murray, C. B.; Norris, D. J.; Bawendi, M. G. Synthesis and Characterization of Nearly Monodisperse CdE (E = S, Se, Te) Semiconductor Nanocrystallites. *J. Am. Chem. Soc.* **1993**, *115*, 8706–8715.
3. Katari, J. E. B.; Colvin, V. L.; Alivisatos, A. P. X-ray Photoelectron Spectroscopy of CdSe Nanocrystals with Applications to Studies of the Nanocrystal Surface. *J. Phys. Chem.* **1994**, *98*, 4109–4117.
4. Trentler, T. J.; Hickman, K. M.; Goel, S. C.; Viano, A. M.; Gibbons, P. C.; Buhro, W. E. Solution−Liquid−Solid Growth of Crystalline III−V Semiconductors: An Analogy to Vapor−Liquid−Solid Growth. *Science* **1995**, *270*, 1791–1794.

5. Yu, H.; Buhro, W. E. Solution−Liquid−Solid Growth of Soluble GaAs Nanowires. *Adv. Mater.* **2003**, *15*, 416–418.
6. Yu, H.; Li, J. B.; Loomis, R. A.; Wang, L. W.; Buhro, W. E. Two-*versus* Three-Dimensional Quantum Confinement in Indium Phosphide Wires and Dots. *Nat. Mater.* **2003**, *2*, 517–520.
7. Yu, H.; Loomis, R. A.; Gibbons, P. C.; Wang, L. W.; Buhro, W. E. Cadmium Selenide Quantum Wires and the Transition from 3D to 2D Confinement. *J. Am. Chem. Soc.* **2003**, *125*, 16168–16169.
8. Grebinski, J. W.; Richter, K. L.; Zhang, J.; Kosel, T. H.; Kuno, M. Synthesis and Charcterization of Au/Bi Core/Shell Nanocrystals: A Precursor toward II−VI Nanowires. *J. Phys. Chem. B* **2004**, *108*, 9745–9751.
9. Grebinski, J. W.; Hull, K. L.; Zhang, J.; Kosel, T. H.; Kuno, M. Solution-Based Straight and Branched CdSe Nanowires. *Chem. Mater.* **2004**, *16*, 5260–5272.
10. Hull, K. L.; Grebinski, J. W.; Kosel, T. H.; Kuno, M. Induced Branching in Confined PbSe Nanowires. *Chem. Mater.* **2005**, *17*, 4416–4425.
11. Puthussery, J.; Kosel, T. H.; Kuno, M. Facile Synthesis and Size Control of II−VI Nanowires Using Bismuth Salts. *Small* **2009**, *5*, 1112–1116.
12. Holmes, J. D.; Johnston, K. P.; Doty, R. C.; Korgel, B. A. Control of Thickness and Orientation of Solution-Grown Silicon Nanowires. *Science* **2000**, *287*, 1471–1473.
13. Heitsch, A. T.; Fanfair, D. D.; Tuan, H.-Y.; Korgel, B. A. Solution−Liquid−Solid (SLS) Growth of Silicon Nanowires. *J. Am. Chem. Soc.* **2008**, *130*, 5436–5437.
14. Li, Z.; Kornowski, A.; Myalitsin, A; Mews, A. Formation and Function of Bismuth Nanocatalysts for the Solution−Liquid−Solid Synthesis of CdSe Nanowires. *Small* **2008**, *4*, 1698–1702.
15. Leatherdale, C. A.; Woo, W.-K.; Mikulec, F. V.; Bawendi, M. G. On the Absorption Cross Section of CdSe Nanocrystal Quantum Dots. *J. Phys. Chem. B* **2002**, *106*, 7619–7622.
16. Yu, W. W.; Qu, L.; Guo, W; Peng, X. Experimental Determination of the Extinction Coefficient of CdTe, CdSe, and CdS Nanocrystals. *Chem. Mater.* **2003**, *15*, 2854–2860.
17. Yu, P.; Beard, M. C.; Ellingson, R. J.; Ferrere, S.; Curtis, C.; Drexler, J.; Luiszer, F.; Nozik, A. J. Absorption Cross-Section and Related Optical Properties of Colloidal InAs Quantum Dots. *J. Phys. Chem. B* **2005**, *109*, 7084–7087.
18. Protasenko, V.; Bacinello, D.; Kuno, M. Experimental Determination of the Absorption Cross-Section and Molar Extinction Coefficient of CdSe and CdTe Nanowires. *J. Phys. Chem. B* **2006**, *110*, 25322–25331.
19. Protasenko, V.; Hull, K. L.; Kuno, M. Disorder-Induced Optical Heterogeneity in Single CdSe Nanowires. *Adv. Mater.* **2005**, *17*, 2942–2949.
20. Giblin, J; Protasenko, V.; Kuno, M. Wavelength Sensitivity of Single Nanowire Excitation Polarization Anisotropies Explained through a Generalized Treatment of Their Linear Absorption. *ACS Nano* **2009**, *3*, 1979–1987.
21. Berciaud, S.; Cognet, L.; Blab, G. A.; Lounis, B. Photothermal Heterodyne Imaging of Individual Nonfluorescent Nanoclusters and Nanocrystals. *Phys. Rev. Lett.* **2004**, *93*, 257402-1–257402-4.
22. Berciaud, S.; Cognet, L.; Tamarat, P.; Lounis, B. Observation of Intrinsic Size Effects in the Optical Response of Individual Gold Nanoparticles. *Nano Lett.* **2005**, *5*, 515–518.
23. Berciaud, S.; Cognet, L.; Lounis, B. Photothermal Absorption Spectroscopy of Individual Semiconductor Nanocrystals. *Nano Lett.* **2005**, *5*, 2160–2163.
24. Berciaud, S.; Cognet, L.; Poulin, P.; Weisman, R. B.; Lounis, B. Absorption Spectroscopy of Individual Single-Walled Carbon Nanotubes. *Nano Lett.* **2007**, *7*, 1203–1207.
25. Berciaud, S.; Cognet, L.; Lounis, B. Luminescence Decay and the Absorption Cross Section of Individual Single-Walled Carbon Nanotubes. *Phys. Rev. Lett.* **2008**, *101*, 077402−1−077402−4.
26. Berciaud, S.; Lasne, D.; Blab, G. A.; Cognet, L.; Lounis, B. Photothermal Heterodyne Imaging of Individual Metallic Nanoparticles: Theory *versus* Experiment. *Phys. Rev. B* **2006**, *73*, 045424-1045424−8.
27. Puthussery, J; Lan, A.; Kosel, T. H.; Kuno, M. Band-Filling of Solution-Synthesized CdS Nanowires. *ACS Nano* **2008**, *2*, 357–367.
28. Kuno, M.; Ahmad, O.; Protasenko, V.; Bacinello, D.; Kosel, T. H. Solution-Based Straight and Branched CdTe Nanowires. *Chem. Mater.* **2006**, *18*, 5722–5732.
29. Glennon, J. J.; Tang, R.; Buhro, W. E.; Loomis, R. A. Synchronous Photoluminescence Intermittency (Blinking) along Whole Semiconductor Quantum Wires. *Nano Lett.* **2007**, *7*, 3290–3295.
30. Wang, F.; Dong, A; Sun, J.; Tang, R.; Yu, H; Buhro, W. E. Solution−Liquid−Solid Growth of Semiconductor Nanowires. *Inorg. Chem.* **2006**, *45*, 7511–7521.
31. Kukura, P.; Celebrano, M.; Renn, A.; Sandoghdar, V. Imaging a Single Quantum Dot When It Is Dark. *Nano Lett.* **2009**, *9*, 926–929.
32. Henglein, A. Radiolytic Preparation of Ultrafine Colloidal Gold Particles in Aqueous Solution: Optical Spectrum, Controlled Growth, and Some Chemical Reactions. *Langmuir* **1999**, *15*, 6738–6744.
33. Knight, M. W.; Grady, N. K.; Bardhan, R.; Hao, F.; Nordlander, P.; Halas, N. J. Nanoparticle-Mediated Coupling of Light into a Nanowire. *Nano Lett.* **2007**, *7*, 2346–2350.
34. Johnson, P. B.; Christy, R. W. Optical Constants of the Noble Metals. *Phys. Rev. B* **1972**, *6*, 4370–4379.
35. Muskens, O. L.; Bachelier, G.; Del Fatti, N.; Vallee, F.; Brioude, A.; Jiang, X. C.; Pileni, M. P. Quantitative Absorption Spectroscopy of a Single Gold Nanorod. *J. Phys. Chem. C* **2008**, *112*, 8917–8921.
36. Lan, A. D.; Giblin, J.; Protasenko, V.; Kuno, M. Excitation and Photoluminescence Polarization Anisotropy of Single CdSe Nanowires. *Appl. Phys. Lett.* **2008**, *92*, 183110-1–183110-3.
37. Wang, J.; Gudiksen, M. S.; Duan, X.; Cui, Y.; Lieber, C. M. Highly Polarized Photoluminescence and Photodetection from Single Indium Phosphide Nanowires. *Science* **2001**, *293*, 1455–1457.
38. Bohren, C. F.; Huffman, D. R. *Absorption and Scattering of Light by Small Particles*; John Wiley & Sons, Inc.: New York 1983; p 73.
39. Palik, E. D. *Handbook of Optical Constants of Solids II*; Academic Press: San Diego, CA, 1998; pp 559−578.
40. Hwang, J.; Moerner, W. E. Interferometry of a Single Nanoparticle using the Gouy Phase of a Focused Laser Beam. *Opt. Commun.* **2007**, *280*, 487–491.
41. Arbouct, A.; Christofilos, D.; Del Fatti, N.; Vallée, F.; Huntzinger, J. R.; Arnaud, L.; Billaud, P.; Boyer, M. Direct Measurement of the Single-Metal-Cluster Optical Absorption. *Phys. Rev. Lett.* **2004**, *93*, 127401-1–127401-4.